

A Novel Electrochemical Sensor Based on SH- β -cyclodextrin Functionalized Gold Nanoparticles/Reduced-Graphene Oxide Nanohybrids for Ultrasensitive Electrochemical Sensing of Acetaminophen and Ofloxacin

Zhiming Jiang, Guangyu Li, Mingxiao Zhang*

School of Chemistry and Chemical Engineering, Southwest University, Chong Qing 400715, PR China

*E-mail: pclab@swu.edu.cn

Received: 2 July 2016 / Accepted: 5 September 2016 / Published: 12 May 2017

A novel electrochemical sensor based on SH- β -cyclodextrin functionalized gold nanoparticles/reduced-graphene oxide (SH- β -CD/AuNPs/rGO) nanohybrids for ultrasensitive electrochemical sensing of acetaminophen and ofloxacin was developed. A SH- β -CD/AuNPs/rGO nanohybrids modified glassy carbon electrode (GCE) was successfully fabricated by one-pot electrochemical synthesis. The morphology and structure of the SH- β -CD/AuNPs/rGO/GCE were investigated by scanning electron microscopy (SEM) and fourier transform infrared (FT-IR). The conditions for the SH- β -CD/AuNPs/rGO/GCE preparation and the determination of acetaminophen and ofloxacin were discussed in detail. Under the optimized conditions, the differential pulse voltammograms (DPV) exhibited that the oxidation peak currents were linearly proportional to their concentrations in the range of 0.05–100 μM for acetaminophen and 0.01–10 μM for ofloxacin with high sensitivities of 0.26 $\mu\text{A } \mu\text{M}^{-1}$ for acetaminophen and 0.28 $\mu\text{A } \mu\text{M}^{-1}$ for ofloxacin, respectively. The detection limits of acetaminophen and ofloxacin were 0.03 μM and 0.008 μM ($S/N=3$), respectively. This sensor was successfully used to detect the concentrations of acetaminophen and ofloxacin in pharmaceutical formulations and human urine samples. The results suggest that the SH- β -CD/AuNPs/rGO nanohybrids has a potential application for electroanalytical sensor.

Keywords: Electrochemical sensor; SH- β -cyclodextrin; gold nanoparticles; reduced-graphene oxide; acetaminophen; ofloxacin

1. INTRODUCTION

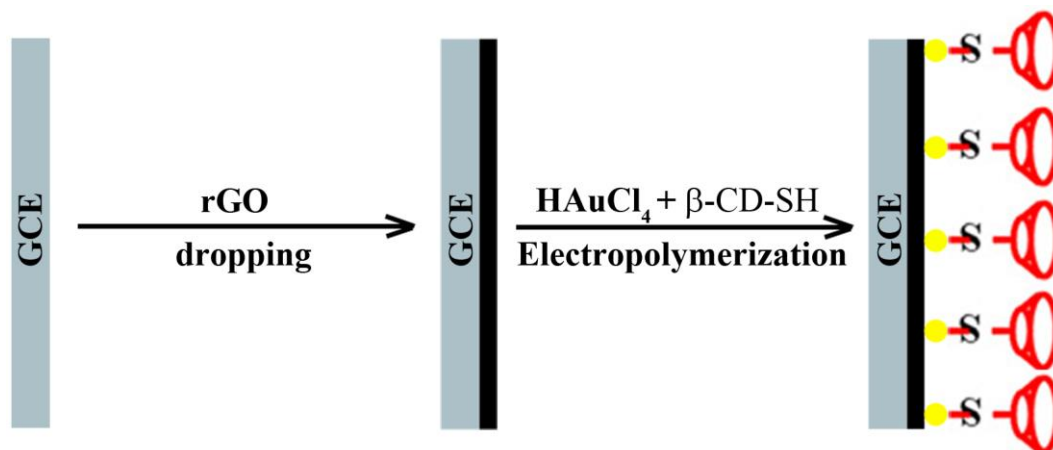
Acetaminophen (AC) is employed to cure arthralgia, neuralgia, cephalagra, cancer pain, headache, backache and postoperative pain [1-3]. However, acute overdoses of AC can cause the liver and kidney damage [4]. Ofloxacin (OFL) is a member of synthetic quinolones which has a broad-

spectrum antibacterial activity against both gram-negative and gram-positive bacteria [5,6]. OFL has been widely used for the treatment of respiratory, urogenital, and gastrointestinal infections [7]. AC and OFL both play important analgesic and antibacterial roles in daily life. There is a considerable probability of coinstantaneous intake of AC and OFL in daily life. However, extensive or unreasonable use of AC and OFL can increase the damage for human health. Therefore, It is essential to establish a sensitive method for the simultaneous determination of AC and OFL.

Several analytical methods, such as high performance liquid chromatography [8,9], spectrofluorometry [10,11] and capillary electrophoresis [12,13] have been used for the detection of AC and OFL. Compared with the above analytical methods, electrochemical techniques possess the advantages of high sensitivity, easy simplicity, low cost and rapid response. Hence, in recent years electrochemical techniques have been proposed for the detection of AC [14-21] and OFL [22-26].

Cyclodextrins (CDs) have the ability of allowing small hydrophobic molecules inside their cavities [27,28]. The unique structural properties of CDs can bind the molecules to form stable host-guest inclusion complexes with high molecular selectivity [29,30]. Noble metal nanomaterials have attracted considerable attention because of their catalytic properties [31,32]. The surface energies increase with decreased noble metal particle size, leading to serious aggregation of small particles [33,34]. The metal particles must be anchored to suitable supports to overcome this aggregation [35,36]. The reduced graphene oxide (rGO), obtained by reduction of graphene oxide (GO), is considered an ideal platform for growing or anchoring functional nanomaterials [36,37]. The reduced graphene oxide (rGO) has the unique properties such as high specific surface area and high chemical stability [38-40].

In the present study, SH- β -CD/AuNPs/rGO nanohybrids was fabricated by one-pot cyclic voltammetry of the mixed solution of HAuCl_4 and SH- β -CD for the first time, and then applied successfully in sensitive and simultaneous electrochemical detection of acetaminophen and ofloxacin. The gold nanoparticles obtained by electrochemical reduction of HAuCl_4 were anchored onto rGO/GCE and the SH- β -CD was simultaneously attached to the surface of the AuNPs/rGO/GCE with the aid of the covalent bonding between Au and thiol. The designed electrochemical sensing platform is shown in Scheme 1.



Scheme 1. Schematic illustration of the fabrication procedures of the SH- β -CD/AuNPs/rGO/GCE.

2. EXPERIMENTAL

2.1. Reagents and apparatus

Reduced graphene oxide (rGO) was purchased from Nanjing XFNANO Materials Tech Co., Ltd. (Nanjing, China). Gold chloride ($\text{HAuCl}_4 \cdot 3\text{H}_2\text{O}$, 99%) and acetaminophen were purchased from Aladdin Chemical Reagent Co., Ltd. (Shanghai, China). Thiol- β -cyclodextrin (SH- β -CD) was purchased from Shandong Binzhou Zhiyuan Bio-Technology Co., Ltd. (Shandong, China). Ofloxacin, moxifloxacin, gatifloxacin, ciprofloxacin and norfloxacin were purchased from Wuhan Yuancheng Gongchuang Technology Co., Ltd. (China). All the other reagents were of analytical grade and used as received without any purification. Ofloxacin Tablets and Compound Ganmaoling Granules were purchased from the drugstore. Fresh urine samples obtained from healthy person were supplied by Southwest University Hospital. Ultrapure water purified from the Millipore water purification system was used throughout the experiments.

Electrochemical experiments were performed on a LK 2006AZ electrochemical workstation (Tianjin Lanlike Co., Ltd., China), with a conventional three-electrode system including the modified GCE as working electrode, a Pt wire counter electrode and a saturated calomel electrode (SCE) reference electrode. The scanning electron micrograph (SEM) measurement was carried out on scanning electron microscope (JSM-6510, Japan). FT-IR spectra for the various samples were recorded on a Bruker Tensor 27.

2.2. Preparation of the reduced graphene oxide-modified electrode

The bare GCE (3 mm in diameter) was polished with $0.05 \mu\text{m}$ Al_2O_3 slurry, and rinsed ultrasonically with 1:1 HNO_3 , ethanol and ultrapure water respectively. Two microliters of the reduced graphene oxide suspension (1.0 mg/mL) was dropped onto the surface of the GCE and dried in the vacuum oven at 60°C for 1 h.

2.3. Construction of the AuNPs/rGO/GCE, SH- β -CD/rGO/GCE and SH- β -CD/AuNPs/rGO/GCE

The rGO/GCE was immersed in 10.0 mL phosphate buffer solution (pH = 6.0) containing 0.10 mM HAuCl_4 and 0.10 mM SH- β -CD and subjected to 15 scans of CV in the potential range of -0.8 to 1.3 V at 100 mV s^{-1} . Eventually, the as-prepared electrode (SH- β -CD/AuNPs/rGO/GCE) was rinsed carefully with double distilled water for further use. For comparison, the AuNPs/rGO/GCE and SH- β -CD/rGO/GCE were prepared by the same procedure but without the addition of SH- β -CD and AuNPs, respectively.

2.4. Electrochemical characterization and measurements

The EIS characterization of different modified electrodes was performed in a solution of 5.0 mM $\text{K}_3[\text{Fe}(\text{CN})_6]/\text{K}_4[\text{Fe}(\text{CN})_6]$ (1:1) containing 0.10 M KCl. The following parameters were employed

for analytical application. DPV conditions: pulse amplitude 50 mV, pulse width 50 ms, interval time 0.2 s. CV conditions: scan rate 100 mV s⁻¹. All electrochemical experiments were carried out at about 25 °C.

2.5. Preparation and determination of real samples

Ten tablets of ofloxacin drug were accurately weighed. A quantity equivalent to one tablet was weighed, dissolved into double distilled water and transferred to a 100 mL volumetric flask, and diluted to the mark with double distilled water. The resulting solution was centrifuged at 5000 rpm; then, the supernatant was collected and diluted to 100 mL and used as a stock solution of the sample. Compound Ganmaoling Granules are composed of acetaminophen, chlorpheniramine maleate, caffeine and some traditional Chinese medicine. One bag was placed in a 1000 mL volumetric flask and diluted with ultrapure water to scale. The two samples were stored at 4 °C, when not in use. Urine samples were spiked with known concentration of acetaminophen and ofloxacin, centrifuged (3000 rpm, 10 min) to removal of proteins and diluted with 0.10 M PBS (pH 7.0).

3. RESULTS AND DISCUSSION

3.1. Characterization of the morphology of the modified electrodes

3.1.1. SEM images

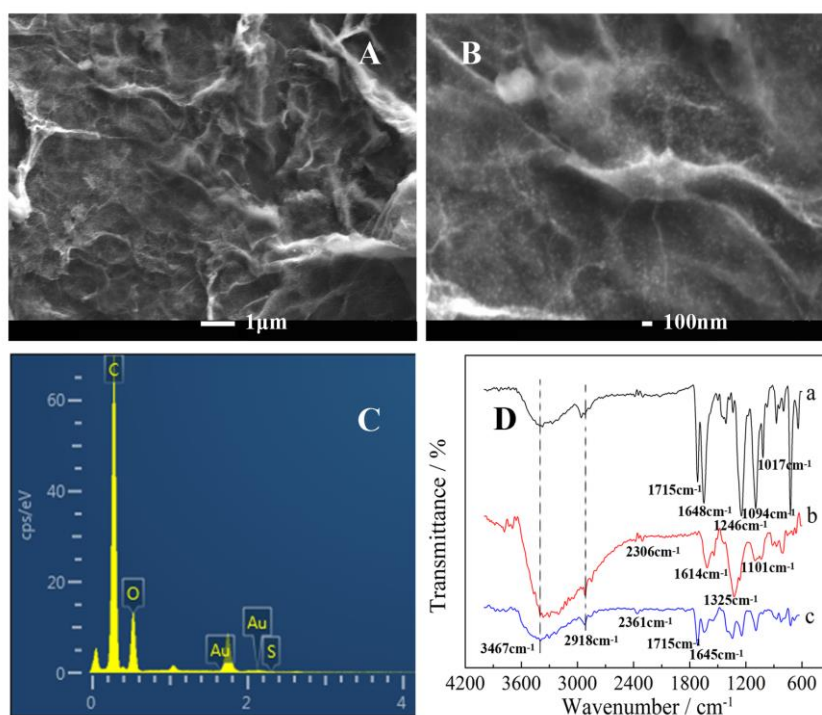


Figure 1. SEM image (A, B) and EDX pattern (C) of rGO/AuNPs/β-CD-SH. FT-IR spectra (D) of GCE/rGO (a), GCE/β-CD-SH (b) and GCE/rGO/AuNPs/β-CD-SH (c).

The morphology of the rGO/AuNPs/ β -CD-SH hybrids was characterized by the scanning electron microscopy (SEM). Fig. 1A shows the SEM image of the rGO/AuNPs/ β -CD-SH hybrids and the Fig. 1B is the related SEM image in higher magnification. The SEM image of the rGO/AuNPs/ β -CD-SH hybrids revealed a wrinkled texture that is associated with the presence of β -CD-SH. In the rGO/AuNPs/ β -CD-SH composite, Au particles are clearly observed to be distributed between the rGO and β -CD-SH (Fig. 1B). Fig. 1C shows the energy-dispersive X-ray (EDX) pattern of rGO/AuNPs/ β -CD-SH hybrids. The results from Fig. 1C indicate that C, O, Au and S exist in the rGO/AuNPs/ β -CD-SH hybrids.

3.1.2. FT-IR spectroscopy

Fig. 1D shows the FT-IR spectra of the GCE/rGO (a), GCE/ β -CD-SH (b) and GCE/rGO/AuNPs/ β -CD-SH (c). The peaks of curve c that are observed at 3467, 2918, 2361, 1715, 1645, 1343, and 1244 (1092) cm^{-1} correspond to the stretching vibrations of O–H, C–H, S–H, C=O, C=C, C–O and C–OH. The FT-IR spectrum of the GCE/rGO/AuNPs/ β -CD-SH (c) exhibits β -CD-SH absorption features of the coupled C–O stretching / O–H bending vibrations at 1101 (1036) cm^{-1} / 1325 (1264) cm^{-1} , C–H stretching vibrations at 2918 cm^{-1} , and O–H stretching vibrations at 3467 cm^{-1} . The presence of these peaks confirmed that the β -CD-SH molecules were attached to the surface of the GCE/rGO/AuNPs [41,51].

3.2. Electrochemical performance of the modified electrodes

Fig. 2A shows the typical EIS measurements of the bare GCE (a), GCE/rGO (b), GCE/rGO/AuNPs (c) and GCE/rGO/AuNPs/ β -CD-SH (d), respectively. After dropping rGO on the surface of electrode, the electron transfer resistance increased, which indicated that the rGO has larger obstruction effect and thus hindered the charge transfer. When AuNPs were electropolymerized on GCE/rGO, the electron transfer resistance decreased sharply, illustrated that AuNPs were able to decrease the electrical resistance and promote the charge transfer. The electron transfer resistance increased with the modification of β -CD-SH, which can be attributed to the poor electrical conductivity of SH- β -CD [26]. Fig. 2B shows the CVs of 5.0 mM $[\text{Fe}(\text{CN})_6]^{3-/4-}$ containing 0.10 M KCl at bare GCE (a), rGO/GCE (b), AuNPs/rGO/GCE (c) and SH- β -CD/AuNPs/rGO/GCE (d). Compared with the bare GCE, the current intensities decrease with higher ΔE_p observed at rGO/GCE, which is attributed to some oxygen-containing groups of rGO. The Fe(III)/Fe(II) redox couple is highly active on AuNPs/rGO/GCE with increased peak current response with low ΔE_p . This is because of the high conductivity of AuNPs/rGO composite [42]. Whereas the ΔE_p increased at SH- β -CD/AuNPs/rGO/GCE with response current slightly lower than that at AuNPs/rGO/GCE, which can be attributed to the poor electrical conductivity of SH- β -CD [26]. These results further indicated the successful modification of SH- β -CD/AuNPs/rGO nanohybrids on the GCE.

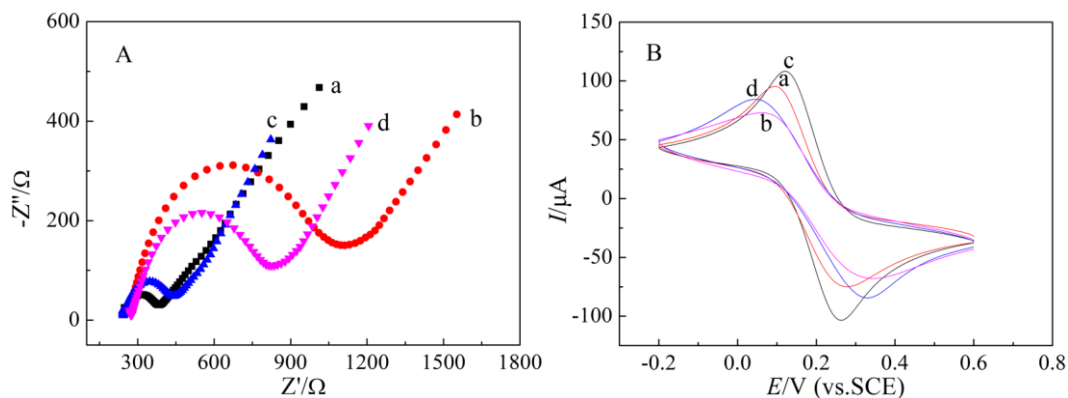


Figure 2. EIS (A) and CVs (B) of different modified electrodes in 5.0 mM $K_3[Fe(CN)_6]/K_4[Fe(CN)_6]$ containing 0.10 M KCl: GCE (a), GCE/rGO (b), GCE/rGO/AuNPs (c), GCE/rGO/AuNPs/ β -CD-SH (d).

3.3. Electrochemical behavior of acetaminophen and ofloxacin at the modified electrodes

3.3.1. CVs of the modified electrodes to AC and OFL

Figure 3 shows cyclic voltammograms (CVs) response of 1.0 μ M AC and 1.0 μ M OFL mixture on the surface of SH- β -CD/AuNPs/rGO/GCE (e) in 0.10 M PBS (pH = 5.0). In contrast, bare GCE (a), AuNPs/rGO/GCE (b), SH- β -CD/rGO/GCE (c), and SH- β -CD/AuNPs/GCE (d) were also investigated. The voltammogram signal of AC on the bare GCE displays just one small anodic peak at 0.45 V. However, the voltammogram signal of AC on the modified electrodes displays two reversible peaks at 0.45 V and 0.35 V. This phenomenon is consistent with the literature report [43]. One anodic peak appears at 0.90 V on bare GCE and the modified electrodes for OFL. Furthermore, there is a reduction peak around 0.6 V at the AuNPs/rGO/GCE (b). The presence of AuNP in acidic media, usually results in characteristic reduction peak around 0.6 V [44]. Whereas the characteristic peak for Au disappears at the SH- β -CD/AuNPs/rGO/GCE, which can be attributed to the SH- β -CD. The SH- β -CD was attached to the surface of the AuNPs/rGO/GCE. After modified with SH- β -CD, the peak current of SH- β -CD/AuNPs/rGO/GCE for AC and OFL shows a increasement compared with the AuNPs/rGO/GCE. This phenomenon results from the hydrophobic cavity that allows SH- β -CD to accelerate the absorption of AC and OFL [45]. AuNPs is a good electrocatalyst for AC and OFL oxidization by the comparison of SH- β -CD/rGO/GCE and SH- β -CD/AuNPs/rGO/GCE. The oxidation peak currents of AC and OFL increase at SH- β -CD/AuNPs/rGO/GCE compared with the SH- β -CD/AuNPs/GCE. rGO in the modified layer is considered an platform for growing or anchoring metal nanoparticles to overcome the aggregation of metal nanoparticles [42]. The peak current value of DPV for AC and OFL using the different electrodes are shown in Table 1. Compared with the other modified electrodes, the oxidation peak current of SH- β -CD/AuNPs/rGO/GCE is the largest.

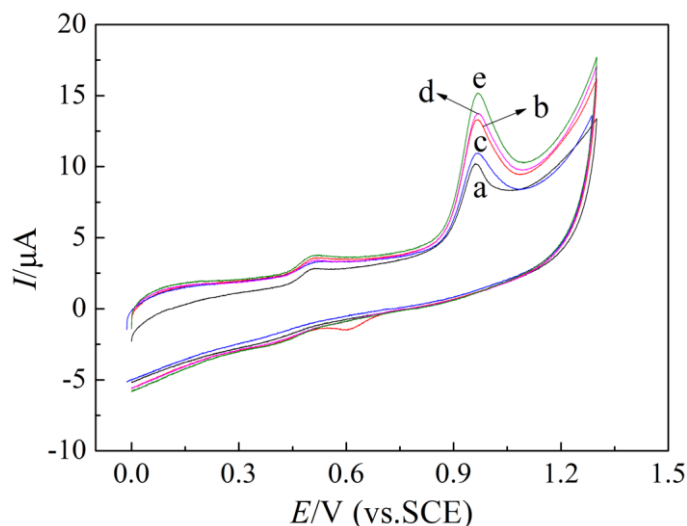


Figure 3. CV obtained at bare GCE (a), AuNPs/rGO/GCE (b), SH-β-CD/rGO/GCE (c), SH-β-CD/AuNPs/GCE (d) and SH-β-CD/AuNPs/rGO/GCE (e) in 0.10 M PBS (pH = 5.0) with 1.0 μM AC and 1.0 μM OFL.

Table 1. Comparison of the different modified electrodes for the determination of 1.0 μM AC and 1.0 μM OFL.

Electrodes	$I_{AC}(\mu A)$	$I_{OF}(\mu A)$
GCE	0.832	4.69
GCE/rGO/AuNPs	1.59	7.29
GCE/rGO/β-CD-SH	1.62	5.24
GCE/AuNPs/β-CD-SH	1.22	6.97
GCE/rGO/AuNPs/β-CD-SH	1.71	7.80

3.3.2 The effect of scan rate

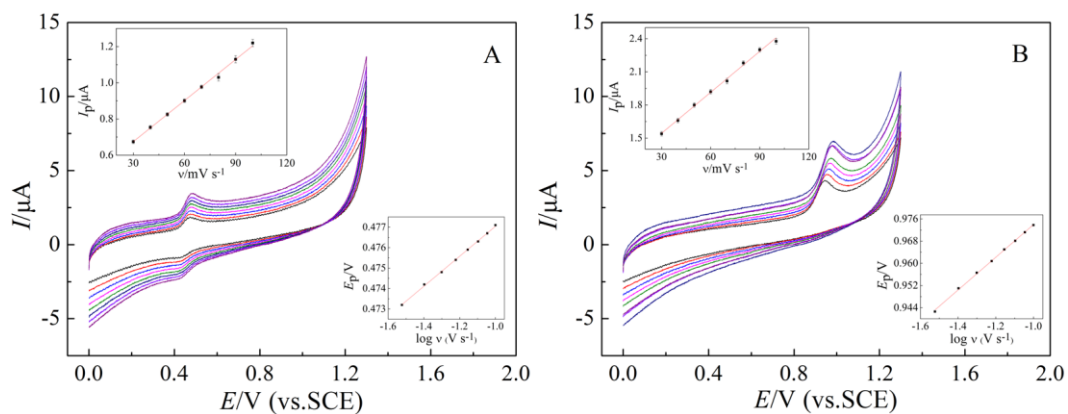


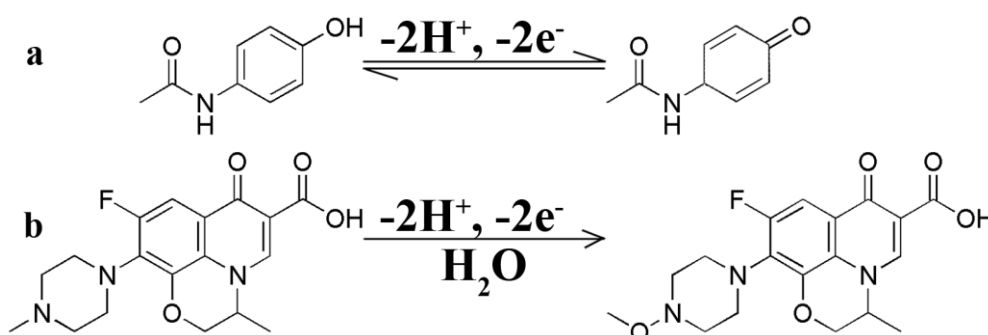
Figure 4. CVs of SH-β-CD/AuNPs/rGO/GCE in 0.10 M PBS (pH = 5.0) with 1.0 μM AC (A) and 1.0 μM OFL (B) at scan rate of 30 to 100 mV s⁻¹. Insets are linear relationships of v vs. I_p and $\log v$ vs. E_p .

Figure 4 shows the effect of scan rate (ν) in 1.0 μM AC and 1.0 μM OFL at SH- β -CD/AuNPs/rGO/GCE by cyclic voltammetry (CV). The linear relationship between the oxidation peak currents and scan rate in the range of 30–100 mV s^{-1} were expressed as $I_p (\mu\text{A}) = 0.00757\nu (\text{mV s}^{-1}) + 0.448$ ($R = 0.998$) and $I_p (\mu\text{A}) = 0.0124\nu (\text{mV s}^{-1}) + 1.17$ ($R = 0.997$) for AC and OFL, respectively. The results indicate that the electrochemical oxidation of AC and OFL at SH- β -CD/AuNPs/rGO/GCE are adsorption-controlled process [45].

The logarithm of scan rate ($\log \nu$) and the anodic peak potential (E_p) have a proportional relationship. The equations of $\log \nu$ and E_p were: $E_p (\text{V}) = 0.0373 \log \nu (\text{V s}^{-1}) + 0.484$ ($R = 0.998$) and $E_p (\text{V}) = 0.0589 \log \nu (\text{V s}^{-1}) + 1.03$ ($R = 0.998$) for AC and OFL, respectively. Therefore, the relationship of E_p and $\log \nu$ satisfied the following equation [46]:

$$E_p = A + [2.303RT / (1-\alpha)nF] \log \nu \quad (1)$$

R , T and F are the gas constant, temperature and Faraday constant, respectively. α is the electron transfer coefficient. n is the number of electrons involved in the rate-controlling step. The values of $(1-\alpha)n$ are calculated to be 1.2 and 1.0 for AC and OFL, respectively. The electron transfer coefficient α is assumed as 0.5 for AC and OFL. The number of transferred electrons is 2. The results are consistent with the reported literatures [23,47]. The inferred mechanisms of AC and OFL oxidation are shown in Scheme 2.



Scheme 2. The electrochemical oxidation mechanisms of AC (a) and OFL (b).

3.4. Optimization of conditions for SH- β -CD/AuNPs/rGO/GCE preparation

3.4.1 Effect of the volume of rGO suspension

As shown in Fig. S1, the AC and OFL current responses increased from 0 to 1.0 μL and then no longer increased with further increase of the rGO volume. A certain amount of rGO on the GCE can overcome the aggregation of AuNPs and promote the electrocatalyst of AuNPs for AC and OFL oxidation [42]. In this experiment, two microliters of the rGO suspension was chosen.

3.4.2 Effect of electropolymerization solution pH

Fig. S2 shows the effect of the pH of the electropolymerization solution on the current response of 1.0 μM AC (Fig. S2A) and 1.0 μM OFL (Fig. S2B). In Fig. S2A, the pH of the

electropolymerization solution has no influence on the oxidation current of AC. In contrast, the oxidation current of OFL increased dramatically with the pH of the electropolymerization solution increasing from 2.6 to 6.0 and decreased after 6.0. The reason may be associated with the molecular structure difference of AC and OFL. Therefore, the pH of the electropolymerization solution was selected as 6.0 in the following investigation.

3.4.3 Scan cycles and scan rate of electropolymerization

Scan cycles and scan rate of electropolymerization would influence the thickness and compactness of the modified materials, respectively [48]. From the results of Fig. S3, higher cycles lead to thicker films for blocking electron transfer between analytes and the electrode. The optimum polymerization cycles was selected as 15. Fig. S4 showed the influence of scan rate on electropolymerization. The oxidation peak current of AC and OFL had little change when the scan rate was less than 100 mV s^{-1} . However, the oxidation peak current of AC and OFL decreased sharply with further increase of the scan rate. An increase of the scan rate to above the threshold value leads to a decrease, probably because of the loose and rough film which decreases the electrode surface conductivity [49]. In order to save the preparation time, the optimum scan rate of electropolymerization was set to be 100 mV s^{-1} .

3.5. Optimization of determination conditions

3.5.1 The optimization of buffer solution pH

Figure S5 illustrates the effect of pH value on the peak potential (E_p) and current (I_p) response of $1.0 \mu\text{M}$ AC and $1.0 \mu\text{M}$ OFL in 0.10 M PBS. The oxidation current of AC reached its peak at pH 5.6 while OFL peaked at pH 5.0. The peak separation between AC and OFL increased at pH 5.0. Thus, pH 5.0 was used for simultaneous determination of AC and OFL.

The oxidation peak potentials of AC and OFL shifted negatively with increasing pH (from 2.6 to 7.4). The phenomenon indicated that the electrochemical oxidation process of AC and OFL was accompanied with protons transport [45]. The relationships between E_p and pH can be expressed by the linear regression equations as: $E_p (\text{V}) = 0.705 - 0.0516 \text{ pH}$ ($R = 0.994$) and $E_p (\text{V}) = 1.18 - 0.0566 \text{ pH}$ ($R = 0.996$) for AC and OFL, respectively. The results confirmed that the number of protons is equal to the transferred electrons in the electrochemical oxidation of AC and OFL [45].

3.5.2 Effect of accumulation

Fig. S6 revealed that the accumulation potential did not affect the oxidation peak currents. Hence, the open-circuit accumulation was performed. The effect of accumulation time was investigated from 0 to 240 s (Fig. S7). The oxidation peak current tended to a constant after 150 s. The results suggested that the amount of AC and OFL at SH- β -CD/AuNPs/rGO/GCE surface tended to a limiting value [50]. In this paper, an accumulation time of 150-s was employed.

3.6. Determination of AC and OFL on SH- β -CD/AuNPs/rGO/GCE

3.6.1 Individual detection of AC and OFL

As shown in Fig. 5, there is a distinct linear relationship between the peak currents of AC and its concentration in the range of 0.05 μM to 100 μM . The regression equation was described as: I_p (μA) = 0.039 + 0.26C (μM) ($R = 0.997$) with the detection limit of 0.03 μM . Fig. 6 showed the detection of OFL. There is a distinct linear relationship between the peak currents of OFL and its concentration in the range of 0.01 μM to 10 μM . The regression equation was described as: I_p (μA) = 0.11 + 0.28C (μM) ($R = 0.997$) with the detection limit of 0.008 μM . Table 2 illustrates the reported electrochemical sensors on detection of AC and OFL over recent years. Compared with these reported sensors, this proposed sensor shows favorable linear range and detection limit.

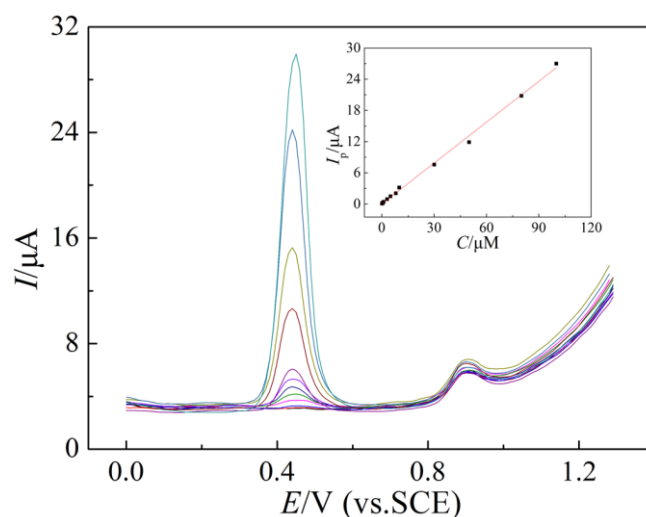


Figure 5. DPVs of different concentrations of AC in the presence of 0.10 μM OFL on SH- β -CD/AuNPs/rGO/GCE in 0.10 M PBS (pH = 5.0). Insert, the plot of the peak current vs. AC concentration.

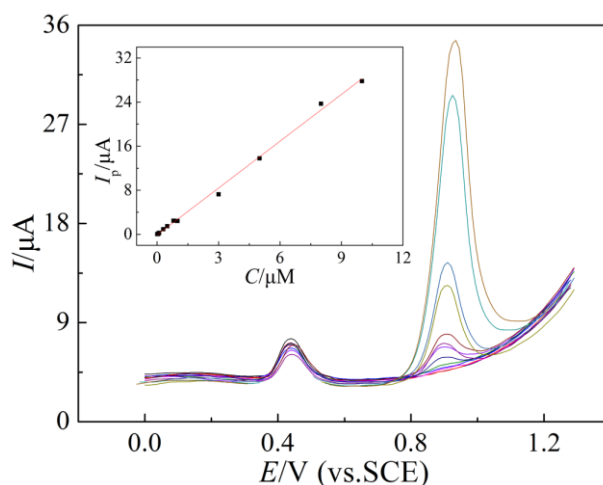


Figure 6. DPVs of different concentrations of OFL on SH- β -CD/AuNPs/rGO/GCE in the presence of 10 μM AC in 0.10 M PBS (pH = 5.0). Insert, the plot of the peak current vs. OFL concentration.

Table 2. Comparisons of the proposed sensor with previous reported electrochemical sensors for AC and OFL determination^a.

Analyses	Modified electrodes	Linear range (μM)	Detection limit (μM)	Reference
AC	GR/GCE	0.1–20	0.032	14
	PANI–MWCNTs/GCE	1.0–100	0.25	15
	ERG/Ni ₂ O ₃ –NiO/GCE	0.04–100	0.02	16
	SWCNT–GNS/GCE	0.05–64.5	0.038	17
	C–Ni/GCE	2.0–230	0.6	18
	Nafion/TiO ₂ –GR/GCE	1.0–100	0.21	19
	Fe ₃ O ₄ /PDDA/GR/GCE	0.1–100	0.037	20
	LNT–CFO/GCE	0.5–901	0.19	21
	SH- β -CD/AuNPs/rGO/GCE	0.05–100	0.03	This work
OFL	HPM α FP/Ppy /GCE	2.0–100	0.065	22
	MWCNTs/Nafion/GCE	0.5–100	0.1	24
	Cysteic acid/CPE	0.06–10	0.02	25
	P- β -CD-l-arg/CPE	0.1–100	0.04	26
	SH- β -CD/AuNPs/rGO/GCE	0.01–10	0.008	This work

^aGR/GCE: graphene modified glassy carbon electrode. PANI–MWCNTs/GCE: polyaniline–multi-walled carbon nanotubes modified glassy carbon electrode. ERG: electrochemically reduced graphene. SWCNT–GNS/GCE: single-walled carbon nanotube–graphene nanosheet hybrid film modified electrode. Fe₃O₄/PDDA/GR/GCE: Fe₃O₄ nanoparticles-coated poly(diallyldimethylammonium chloride)-functionalized graphene nanocomposite film. LNT–CFO/GCE: LaNi_{0.5}–Ti_{0.5}O₃/CoFe₂O₄ nanoparticle-modified electrode. HPM α FP: 1-phenyl-3-methyl-4-(2-furoyl)-5-pyrazolone. Ppy: polypyrrole. P- β -CD-l-arg/CPE: polymerization of β -cyclodextrin (β -CD) and l-arginine (l-arg) modified carbon paste electrode (CPE).

3.6.2 Simultaneous determination of AC and OFL

The linear detection of AC and OFL on SH- β -CD/AuNPs/rGO/GCE is implemented by DPV in 0.10 M PBS (pH = 5.0). The calibration curves of AC and OFL were shown in Fig. 7 with the linear relationship from 0.08 to 10 μM for AC and 0.04 to 10 μM for OFL. The linear equations for AC and OFL were described as following: $I_{\text{AC}} (\mu\text{A}) = 0.28 + 0.050C (\mu\text{M})$ ($R = 0.998$) and $I_{\text{OFL}} (\mu\text{A}) = 3.2 + 0.23C (\mu\text{M})$ ($R = 0.998$).

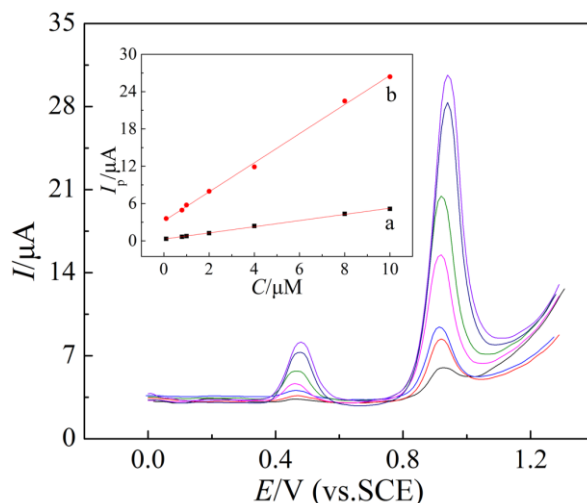


Figure 7. DPV curves obtained from different concentrations of AC and OFL at SH- β -CD/AuNPs/rGO/GCE. Insert, the calibration plots of the oxidation current at SH- β -CD/AuNPs/rGO/GCE versus concentration of AC (a) and OFL (b) under optimal conditions.

3.7 Stability, reproducibility, and anti-interference of the modified electrode

The stability of the modified electrode was tested by 30 successive scan in 10 μ M AC and 10 μ M OFL. The relative standard deviation (RSD) of the oxidation peak currents is 3.27 % and 2.89 % toward AC and OFL, respectively. The results could be ascribed to the long-term stability of SH- β -CD/AuNPs/rGO/GCE.

The reproducibility of SH- β -CD/AuNPs/rGO/GCE was examined by using the same electrode for 6 repetitive measurements of 10 μ M AC and 10 μ M OFL. The relative standard deviation was calculated to be 1.54 % for AC and 2.12 % for OFL. Six different modified electrodes were tested toward the oxidation of 10 μ M AC and 10 μ M OFL. The RSD of the peak current obtained by the six independent electrodes is 3.1 % for AC and 2.8 % for OFL. The results indicated good reproducibility.

The selectivity and anti-interference properties of the proposed sensor were carried out. The results demonstrated that 100-fold concentration of Cu^{2+} , Zn^{2+} , Mg^{2+} , Fe^{3+} , Na^+ , K^+ , Pb^{2+} , Al^{3+} , Ca^{2+} , Fe^{2+} , SO_4^{2-} , Cl^- , NO_3^- , glucose, and urea had no influence on the detection of AC and OFL. The oxidation potentials of ascorbic acid and uric acid were lower than those of AC and OFL in the selected potential range. The structures of moxifloxacin, gatifloxacin, ciprofloxacin and norfloxacin are similar to OFL. Meanwhile, the structure of phenol is similar to AC. The results illustrated that 10-fold of moxifloxacin, gatifloxacin, ciprofloxacin and norfloxacin, and 5-fold phenol hardly caused interference.

3.8 Analysis of real samples

As shown in Table 3, the proposed sensor was used to determine AC and OFL in tablet and human urine samples. The results demonstrated that the proposed sensor is reliable for determination of AC and OFL.

Table 3. Determination of AC and OFL in pharmaceutical formulations and human urine samples ($n = 3$).

No.	Added (μM)		Detected (μM)		Recovery (%)		RSD (%)	
	AC	OFL	AC	OFL	AC	OFL	AC	OFL
Tablets	3.00	2.00	2.94	1.95	98.0	97.5	1.8	1.4
	5.00	4.00	4.96	4.01	99.2	100.3	1.5	1.6
	7.00	6.00	7.03	5.97	100.4	99.5	1.2	1.1
human urine	3.00	2.00	2.98	2.02	99.3	101.0	1.0	1.3
	5.00	4.00	5.01	3.95	100.2	98.8	0.9	1.1
	7.00	6.00	6.98	6.02	99.7	100.3	1.1	1.2

4. CONCLUSION

In this paper, AuNPs/rGO hybrids were prepared and functionalized with SH- β -CD for the first time, and then used successfully to detect AC and OFL. Due to the excellent properties of rGO, AuNPs and SH- β -CD, the SH- β -CD/AuNPs/rGO modified GCE has low detection limit, wide linear range, good reproducibility, and high stability for individual and simultaneous determination of AC and OFL.

ACKNOWLEDGEMENTS

This work was supported by Fundamental Research Funds for the Central Universities (XDJK2016E061).

SUPPORTING INFORMATION

Supplementary data associated with this article can be found in the supporting information.

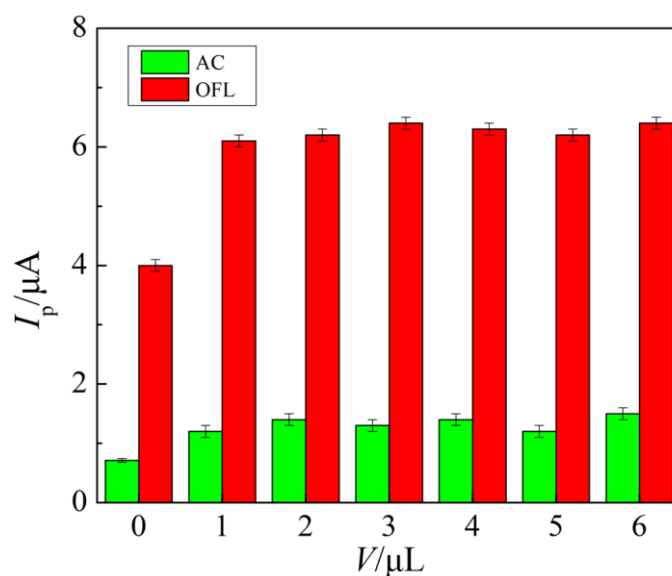


Fig. S1 Effect of the volume of rGO suspension on the peak currents of 1.0 μM AC and 1.0 μM OFL containing 0.10 M PBS (pH = 5.0).

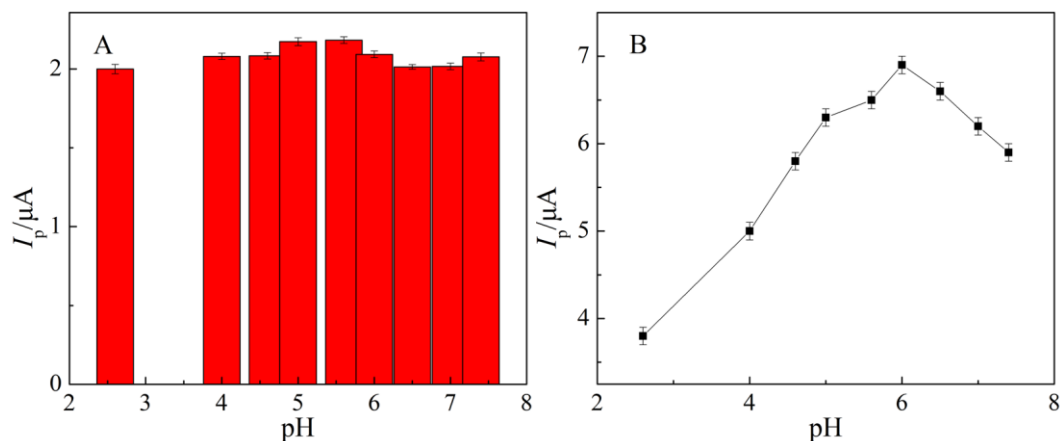


Fig. S2 The pH effect of electropolymerization solution for determination of $1.0 \mu\text{M}$ AC (A) and $1.0 \mu\text{M}$ OFL (B) containing 0.10 M PBS (pH = 5.0).

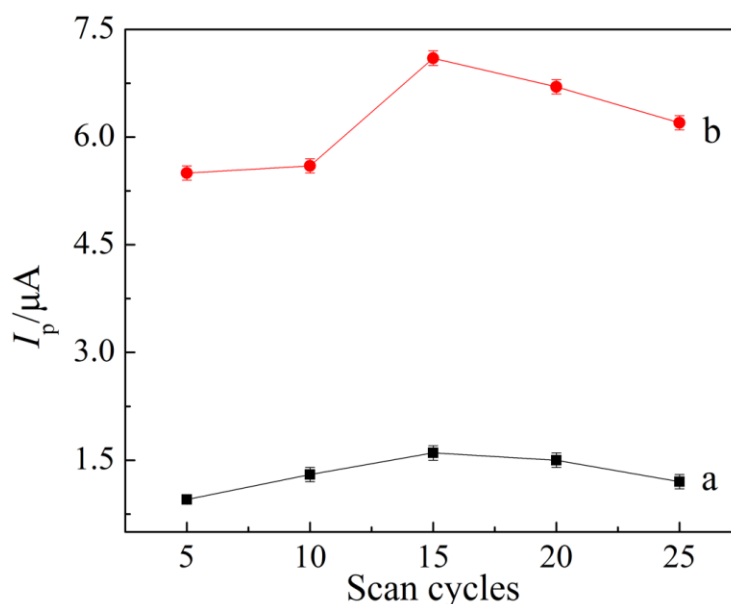


Fig. S3 Optimization of scan cycles for the preparation of SH- β -CD/AuNPs/rGO/GCE in $1.0 \mu\text{M}$ AC (a) and $1.0 \mu\text{M}$ OFL (b) containing 0.10 M PBS (pH = 5.0).

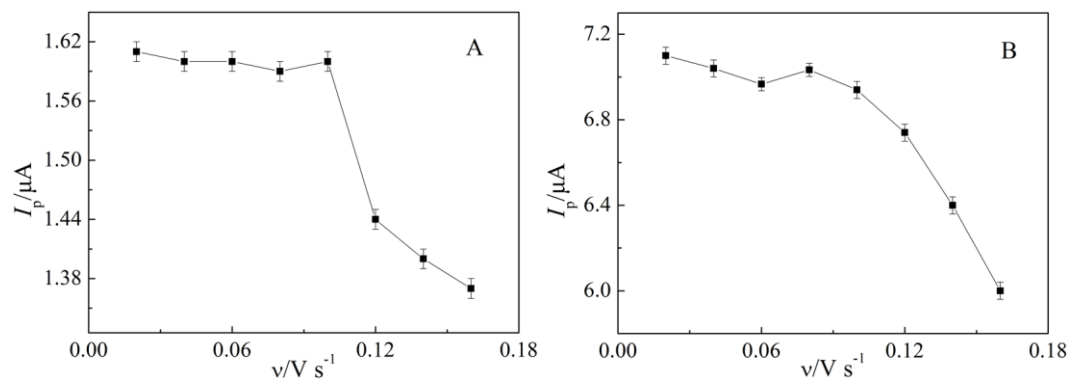


Fig. S4 Optimization of scan rates for the preparation of SH- β -CD/AuNPs/rGO/GCE in $1.0 \mu\text{M}$ AC (A) and $1.0 \mu\text{M}$ OFL (B) containing 0.10 M PBS (pH = 5.0).

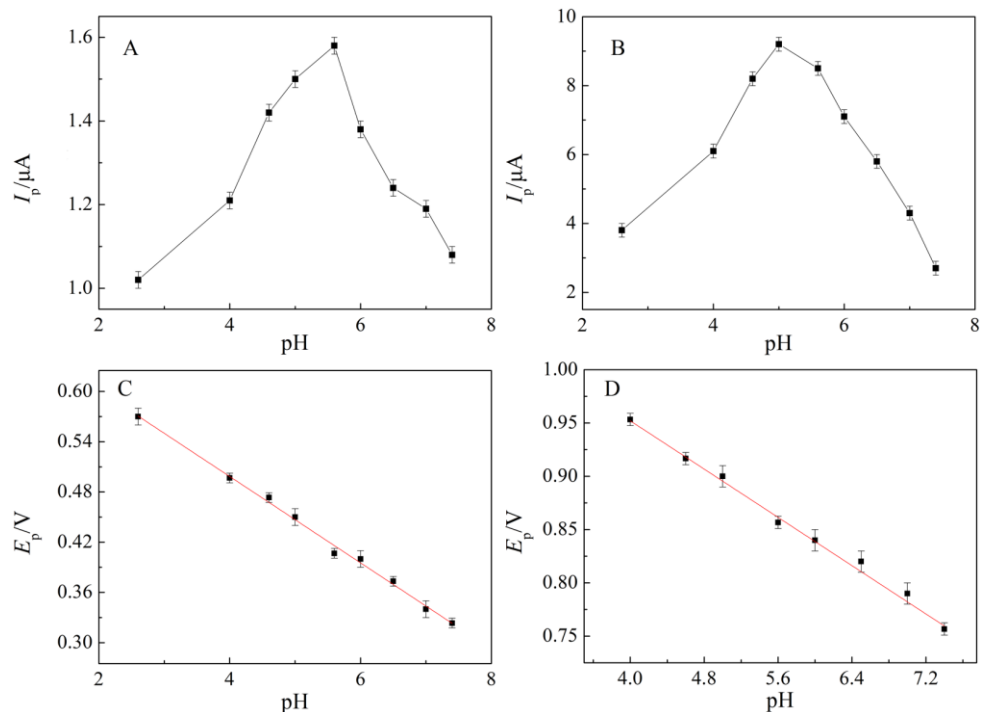


Fig. S5 Effect of pH on the oxidation currents and oxidation potentials of 1.0 μM AC (A, C) and 1.0 μM OFL (B, D).

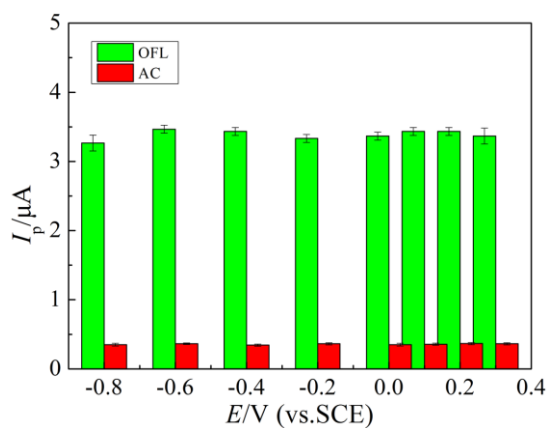


Fig. S6. Effect of accumulation potential on the oxidation peak current of AC and OFL.

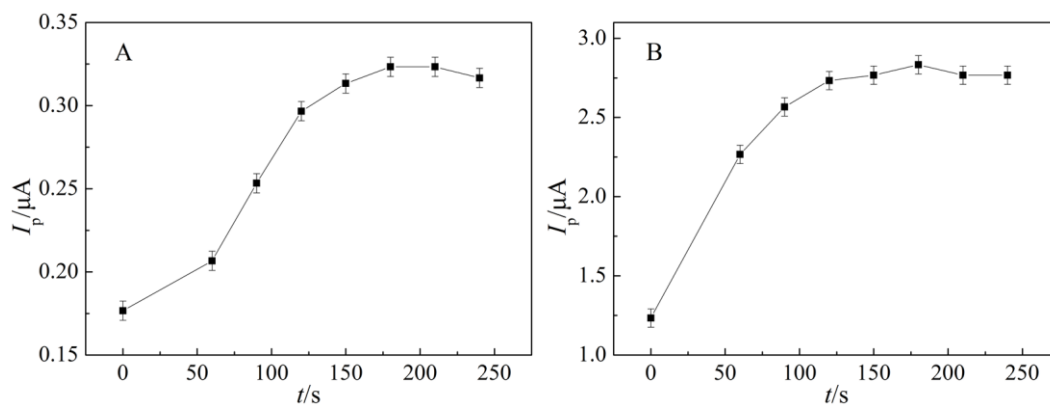


Fig. S7. Influence of accumulation time on the oxidation peak current of AC (A) and OFL (B).

References

1. H. Yin, K. Shang, X. Meng, S. Ai, *Microchim. Acta*, 175 (2011) 39.
2. F. Daly, J. Fountain, L. Murray, A. Graudins, N. Buckley, *Med. J. Aust.*, 188 (2008) 296.
3. N. Tsierkezos, S. Othman, U. Ritter, *Ionics*, 19 (2013) 1897.
4. M. Bosch, A. S´anchez, F. Rojas, C. Ojeda, *J. Pharm. Biomed. Anal.*, 42 (2006) 291.
5. O. Ballesteros, J. V´ılchez, A. Naval´on, *J. Pharm. Biomed. Anal.*, 30 (2002) 1103.
6. K. Sato, Y. Matsuura, M. Inoue, T. Une, Y. Osada, H. Ogawa, S. Mitsuhashi, *Antimicrob. Agents. Chemother.*, 22 (1982) 548.
7. G. Carpini, F. Lucarelli, G. Marrazza, M. Mascini, *Biosens. Bioelectron.*, 20 (2004) 167.
8. A. Mar´ın, C. Barbas, *J. Pharm. Biomed. Anal.*, 35 (2004) 769.
9. G. Cheng, H. Wu, Y. Huang, *Anal. Chim. Acta*, 616 (2008) 230.
10. Y. Ni, C. Liu, S. Kokot, *Anal. Chim. Acta*, 419 (2000) 185.
11. S. Ulu, *Spectrochim. Acta A*, 72 (2009) 1038.
12. H. Modick, A. Schütze, C. Palmke, T. Weiss, T. Bruning, H. Koch, *J. Chromatogr. B*, 925 (2013) 33.
13. B. Awadallah, P. Schmidt, M. Wahl, *J. Chromatogr. A*, 988 (2003) 135.
14. X. Kang, J. Wang, H. Wu, J. Liu, I. Aksayc, Y. Lina, *Talanta*, 81 (2010) 754.
15. M. Li, L. Jing, *Electrochim. Acta*, 52 (2007) 3250.
16. G. Liu, H. Chen, G. Lin, P. Ye, X. Wang, Y. Jiao, X. Guo, Y. Wen, H. Yang, *Biosens. Bioelectron.*, 56 (2014) 26.
17. X. Chen, J. Zhu, Q. Xi, W. S. Yang, *Sensor. Actuat. B*, 161 (2012) 648.
18. S. F. Wang, F. Xie, R. F. Hu, *Sensor. Actuat. B*, 123 (2007) 495.
19. Y. Fan, J. H. Liu, H. T. Lu, Q. Zhang, *Colloid. Surface. B*, 85 (2011) 289.
20. D. B. Lu, Y. Zhang, L. Wang, S. X. Lin, C. M. Wang, X. F. Chen, *Talanta*, 88 (2012) 181.
21. D. X. Ye, Y. H. Xu, L. Q. Luo, Y. P. Ding, Y. L. Wang, X. J. Liu, *J. Solid State Electrochem.*, 16 (2012) 1635.
22. H. Han, J. Li, X. Pang, *Int. J. Electrochem. Sci.*, 8 (2013) 9060.
23. R. Li, S. Lv, J. Shan, J. Zhang, *Ionics*, 21 (2015) 3117.
24. K. Huang, X. Liu, W. Xie, H. Yuan, *Microchim. Acta*, 162 (2008) 227.
25. F. F. Zhang, S. Q. Gu, Y. P. Ding, L. Li, X. Liu, *Bioelectrochemistry*, 89 (2013) 42.
26. F. Zhang, S. Gua, Y. Ding, Z. Zhang, L. Li, *Anal. Chim. Acta*, 770 (2013) 53.
27. Y. Wei, L. Kong, R. Yang, L. Wang, J. Liu, X. Huang, *Chem. Commun.*, 47 (2011) 5340.
28. Z. Liu, A. Zhang, Y. Guo, C. Dong, *Biosens. Bioelectron.*, 58 (2014) 242.
29. Z. Zhang, S. Gu, Y. Ding, M. Shen, L. Jiang, *Biosens. Bioelectron.*, 57 (2014) 239.
30. G. Hu, X. Zhang, P. Gai, X. Zhang, J. Chen, *Nanoscale*, 4 (2012) 5703.
31. J. Farmer, C. Campbell, *Science*, 329 (2010) 933.
32. M. Pang, J. Hu, H. Zeng, *J. Am. Chem. Soc.*, 132 (2010) 10771.
33. R. White, R. Luque, V. Budarin, J. Clark, D. Macquarrie, *Chem. Soc. Rev.*, 38 (2009) 481.
34. X. Chen, G. Wu, J. Chen, X. Chen, Z. Xie, X. Wang, *J. Am. Chem. Soc.*, 133 (2011) 3693.
35. Y. Wang, D. Wilkinson, J. Zhang, *Chem. Rev.*, 111 (2011) 7625.
36. H. Yin, H. Tang, D. Wang, Y. Gao, Z. Tang, *ACS Nano*, 6 (2012) 8288.
37. H. Cong, X. Ren, P. Wang, S. Yu, *ACS Nano*, 6 (2012) 2693.
38. A. Geim, K. Novoselov, *Nat. Mater.*, 6 (2007) 183.
39. M. Pumera, A. Ambrosi, A. Bonanni, E. Chng, H. Poh, *Trends Anal. Chem.*, 29 (2010) 954.
40. V. Singh, D. Joung, L. Zhai, S. Das, S. Khondaker, S. Seal, *Prog. Mater. Sci.*, 56 (2011) 1178.
41. X. Ran, L. Yang, J. Zhang, G. Deng, Y. Li, X. Xie, H. Zhao, C. Li, *Anal. Chim. Acta*, 892 (2015) 85.
42. C. Karuppiyah, K. Muthupandi, S. Chen, M. A. Ali, S. Palanisamy, A. Rajan, P. Prakash, F. Al-Hemaid, B. Lou, *RSC Adv.*, 5 (2015) 31139.

43. B. Jena , S. Percival, B. Zhang, *Anal. Chem.*, 82 (2010) 6737.
44. A. Cernat, M. Tertis, R. Sandulescu, F. Bedioui, A. Cristea, C. Cristea, *Anal. Chim. Acta*, 886 (2015) 16.
45. Y. Hui, X. Ma, X. Hou, F. Chen, J. Yu, *Ionics*, 21 (2015) 1751.
46. L. Jiang, S. Gu, Y. Ding, F. Jiang, Z. Zhang, *Nanoscale*, 6 (2014) 207.
47. H. Ghadimi, R. Tehrani, A. Mohamed Ali, N. Mohamed, S. Ab Ghani, *Anal. Chim. Acta*, 765 (2013) 70.
48. Z. Wang, F. Li, J. Xia, L. Xia, F. Zhang, S. Bi, G. Shi, Y. Xia, J. Liu, Y. Li, L. Xia, *Biosens. Bioelectron.*, 61 (2014) 391.
49. Z. Jiang, G. Li, M. Zhang, *RSC Adv.*, 6 (2016) 32915.
50. A. Abbaspour, A. Noori, *Biosens. Bioelectron.*, 26 (2011) 4674.
51. G. Zhu, P. Gai, Y. Yang, X. Zhang, J. Chen, *Anal. Chim. Acta*, 723 (2012) 33.

© 2017 The Authors. Published by ESG (www.electrochemsci.org). This article is an open access article distributed under the terms and conditions of the Creative Commons Attribution license (<http://creativecommons.org/licenses/by/4.0/>).